UNIVERSITY *of* York

White Rose
university consortium
Universities of Leeds, Sheffield & York

eprints@whiterose.ac.uk
https://eprints.whiterose.ac.uk/

Spatially resolved variations in reflectivity across iron oxide thin films

Chris S. Kelley [a,b], Sarah M. Thompson [a,*], Daniel Gilks [a], James Sizeland [a], Leonardo Lari [c,a], Vlado K. Lazarov [a], Kosuke Matsuzaki [d], Stéphane LeFrançois [e], Gianfelice Cinque [b], Paul Dumas [e]

[a] Department of Physics, University of York, York YO10 5DD, UK
[b] Beamline B22 (MIRIAM), Diamond Light Source, Harwell Science & Innovation Campus, Didcot OX11 0DE, UK
[c] York JEOL Nanocentre, University of York, York YO10 5BR, UK
[d] Secure Materials Center, Materials and Structures Laboratory, Tokyo Institute of Technology, 4259 Nagatsuta, Midori-ku, Yokohama 226-8503, Japan
[e] SMIS Beamline, SOLEIL Synchrotron, L'Orme des Merisiers, Saint-Aubin, Paris, BP 48 91192, France

ABSTRACT

The spin polarising properties of the iron oxide magnetite (Fe_3O_4) make it attractive for use in spintronic devices, but its sensitivity to compositional and structural variations make it challenging to prepare reliably. Infrared microspectroscopy and modelling are used to determine the spatial variation in the chemical composition of three thin films of iron oxide; one prepared by pulsed laser deposition (PLD), one by molecular beam epitaxy (MBE) deposition of iron whilst simultaneously flowing oxygen into the chamber and one by flowing oxygen only once deposition is complete. The technique is easily able to distinguish between films which contain metallic iron and different iron oxide phases as well as spatial variations in composition across the films. The film grown by post-oxidising iron is spatially uniform but not fully oxidised, the film grown by simultaneously oxidising iron showed spatial variation in oxide composition while the film grown by PLD was spatially uniform magnetite.

1. Introduction

The key components of a spintronic device are the spin polarisers and analysers; an important candidate material is the iron oxide magnetite, Fe_3O_4, as it is predicted to be 100% spin polarised at the Fermi energy [1–3]. However, Fe_3O_4 is very sensitive to small variations in chemical composition which can significantly change in the magnetic properties of the material. This leads to a reduction in spin polarisation [4,5] and eventual device failure. It is particularly sensitive to contaminant oxide phases [6], and hence one of the key challenges in the development of Fe_3O_4 based devices is uniform thin film growth. Spatially resolved infrared (IR) reflection microspectroscopy, supported with modelling, has been demonstrated to be an effective non-destructive method of determining the variation of chemical and magnetic properties across Fe_3O_4 thin films [7–9]. Magnetometry and transmission electron microscopy are also employed to support the microspectroscopy conclusions. The new results demonstrate the need for these measurements to understand the growth mechanisms and also the potential of IR microspectroscopy as an effective characterisa-

tion technique. As an exemplar, three deposition methods commonly used to grow Fe_3O_4 thin films were used to prepare three sets of films, IR microspectroscopy was used to measure the variation in oxide composition across the films and models were developed to determine the relative fractions of different oxides present across the samples.

2. Modelling the infrared spectra of iron oxides

The reflectivity, R, of a material is dependent on its complex dielectric function, $\epsilon^*(\omega)$, which itself is a function of the conductivity, σ [10]:

$$R = \left(\frac{\sqrt{\epsilon^*(\omega)} - 1}{\sqrt{\epsilon^*(\omega)} + 1}\right)\left(\frac{\sqrt{\epsilon^*(\omega)} - 1}{\sqrt{\epsilon^*(\omega)} + 1}\right)^* \quad (1)$$

$$\epsilon^*(\omega) = \epsilon(\infty) - \frac{i\sigma}{\epsilon_0 \omega} \quad (2)$$

where ϵ_0 is the vacuum permittivity, ω is the frequency of the incident radiation and $\epsilon(\infty)$ is the DC dielectric parameter. In iron oxides there are several competing conduction processes. There is the Drude contribution, ϵ_{Drude}, which accounts for the metallic conduction [11]:

* Corresponding author.
E-mail address: sarah.thompson@york.ac.uk (S.M. Thompson).

$$\epsilon_{Drude} = \frac{\omega_p^2}{\omega^2 - i\gamma\omega} \tag{3}$$

where $\omega_p^2 = \frac{\widetilde{N}e^2}{m\epsilon_0}$ is the electron plasma frequency, γ is a damping parameter introduced as the inverse of the scattering time $(\gamma = \tau^{-1})$, $\widetilde{N}$ is the number of conduction electrons, m is the electron rest mass and ϵ_0 is the vacuum permittivity. This expression for ϵ_{Drude} assumes that the band structure is flat and resonance free. To account for the resonances in the conductivity, and therefore in the IR spectra, we must include a Lorentz oscillator term to incorporate the phonon contribution, ϵ_{phonon}, to the dielectric function:

$$\epsilon_{phonon} = \sum_{j=1}^{n} \frac{S_j\omega_j^2}{\omega_j - \omega^2 - i\gamma_j\omega_j} \tag{4}$$

where S_j, ω_j and γ_j are the amplitude, resonance frequency and damping constant of the j-th resonance respectively. These terms are sufficient to model maghemite and haematite but magnetite is more complex to model, as other conductivity channels are opened due to its more complex crystal structure. Firstly, there is an additional resonance in the conductivity due to electrons transitioning from the 3d orbital into the 4s orbital, contributing to the conduction, and vice versa. This phenomenon is accounted for by a Lorentz oscillator term, ϵ_{ds}, in an analogous manner to the phonon contribution:

$$\epsilon_{ds} = \frac{S_{ds}\omega_{ds}^2}{\omega_{ds} - \omega^2 - i\gamma_{ds}\omega_{ds}} \tag{5}$$

Table 1
The locations in wavenumbers of characteristic phonon resonances of $\alpha - Fe_2O_3, \gamma - Fe_2O_3$ and Fe_3O_4 [8,17].

Oxide	Formula	Position (cm^{-1})
Haematite	$\alpha - Fe_2O_3$	437
		526
Maghemite	$\gamma - Fe_2O_3$	440
		550
Magnetite	Fe_3O_4	540

where S_{ds}, ω_{ds} and γ_{ds} are the amplitude, resonance frequency and damping constant of the ds resonance respectively. Finally, it is possible for electrons to tunnel between the Fe^{2+} and Fe^{3+} lattice sites across an intermediate O^{2-} site; a phenomenon known as superexchange [12]. Electron–phonon coupling gives rise to a polaron which can "hop" between lattice sites resulting in an increase in conductivity. Hopping has been shown to be the dominant conductivity process in magnetite [7]. Modelling the polaron hopping conductivity is a difficult quantum mechanical problem, it is usually estimated from a large set of fitting parameters (such as those produced by Degiorgi et al. [13]). However, Ahn et al. have shown that the hopping conductivity, $\sigma_{hopping}$, is reasonably constant ($\sim 500 \, \Omega^{-1} \, cm^{-1}$) in the near/mid-IR [14] and so in this case, the hopping contribution to the dielectric function, $\epsilon_{hopping}$, can be estimated as follows:

$$\epsilon_{hopping} = -\frac{4\pi}{i\omega\epsilon_0}\sigma_{hopping} \tag{6}$$

$$= -\frac{7.1 \times 10^{14}}{i\omega} \tag{7}$$

Iron oxides are poor conductors and therefore have large skin depths. This means that, for thin films, the reflectivity contribution from the MgO substrate ϵ_{MgO} must be accounted for in the model. A term to include the possibility of haematite ($\epsilon_{\alpha-Fe_2O_3}$) and maghemite ($\epsilon_{\gamma-Fe_2O_3}$) phase defect contributions must also be included:

$$\epsilon_{MgO} = \epsilon_\infty + \epsilon_{phonon} \tag{8}$$

$$\epsilon_{\alpha-Fe_2O_3} = \epsilon_\infty + \epsilon_{phonon} + \epsilon_{Drude} \tag{9}$$

$$\epsilon_{\gamma-Fe_2O_3} = \epsilon_\infty + \epsilon_{phonon} + \epsilon_{Drude} \tag{10}$$

$$\epsilon_{Fe_3O_4} = \epsilon_\infty + \epsilon_{phonon} + \epsilon_{Drude} + \epsilon_{ds} + \epsilon_{hopping} \tag{11}$$

These expressions for the conductivity are then used to calculate the multilayer reflectivity using the method of McIntyre [15]; as described in more detail in previous work [7,16].

To model the dielectric function of mixed-oxide phases, ϵ_{oxide}, the iron oxide dielectric functions were weighted, where f is the fraction of magnetite present:

$$\epsilon_{oxide} = f\epsilon_{Fe_3O_4} + (1-f)\epsilon_{\alpha/\gamma-Fe_2O_3} \tag{12}$$

(a)   (b)
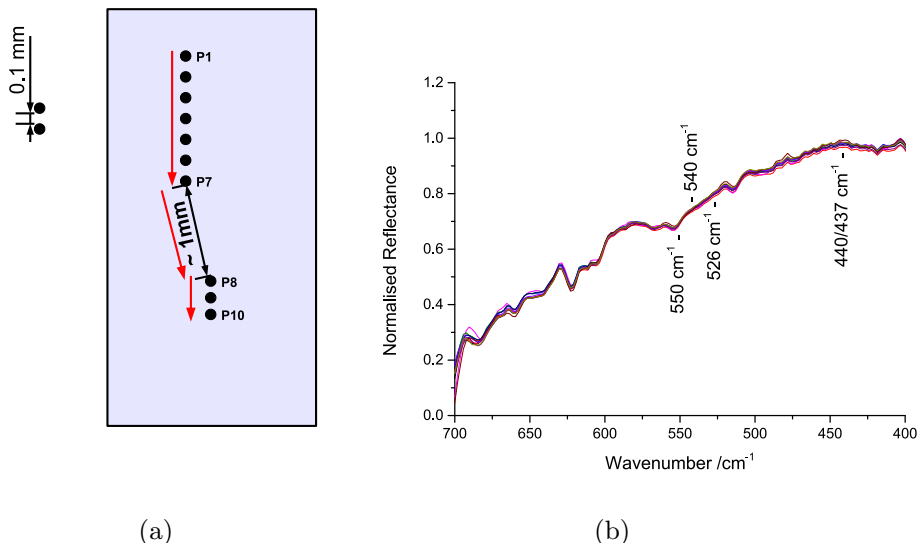
Fig. 1. a) Map of the reflection spectra obtained for the post-oxidised samples. Ten spectra were taken in total in two parts of the sample to test that the spectra obtained were representative of the whole sample. b) Normalised spectra taken at ten points across the post-oxidised Fe_3O_4 thin film that was annealed for 15 min. The normalisation reveals that there are no major spectral features and that the spectra are all flat with some contaminant peaks. This suggests that there is very little oxide formation and the spectrum is being dominated by the strongly reflecting iron. The locations of the phonon peaks of the iron oxides listed in Table 1 are shown to demonstrate their absence.

3. Experimental techniques

IR spectra are typically collected using a Fourier transform infrared (FTIR) spectrometer using a globar source covering the spectral region of interest. Whilst this is an established technique for measuring spectral properties at high spectral resolution, it offers limited spatial resolution due to the diffuse nature of the beam. To obtain the highest spatial resolution, an IR microscope was used at the SMIS beamline at SOLEIL, the French national synchrotron. The collimated radiation from the synchrotron is passed through a Schwarzschild objective before being focussed onto the sample and collected by an MCT detector operating in the range $700 - 400$ cm^{-1}. This combination offers the possibility of collecting IR spectra with a spatial resolution approaching the diffraction limit.

Reflection spectra were taken over the spectral range $700 - 400$ cm^{-1}, with a spot diameter of 20 µm, normalised to a gold reference spectrum. Table 1 shows the expected locations of the three most common iron oxide phonon resonances (haematite, maghemite and magnetite) in this spectral range.

Three growth techniques were used to produce the iron oxide films. The first two employ molecular beam epitaxy (MBE) to deposit iron using an electron beam to evaporate the iron from a metallic source. The base pressure is ultra high vacuum (1×10^{-11} mbar) and the substrate is heated during deposition. In the first method, post-oxidation, a thin film of iron was deposited and then subsequently oxidised in a partial pressure of oxygen. It has been previously observed that the oxidation process is self-limiting and only the top 3 nm of the sample will oxidise [18], therefore it is expected that in thicker films there is a high probability of there being an underlying metallic layer. In the second method, simultaneous oxidation, the iron is deposited in a partial pressure of oxygen at an elevated temperature. The final method is pulsed laser deposition (PLD) in which a high power pulsed laser is used to ablate an oxide target, depositing the oxide material onto the substrate. Subsequent annealing in an oxygen atmosphere was also employed to refine the composition. Specific details of the growth conditions for each of the samples studied are given in the relevant sections.

High resolution transmission electron microscopy (HR-TEM) was used to image the atomic scale structure of the cross-section of the films. The samples were thinned to electron transparency by mechanically polishing and then using an Ar ion mill. The TEM used is a double aberration-corrected JEOL JEM-2200Fs TEM with a 200 kV electron gun, located in the York-JEOL Nanocentre. The room temperature in-plane magnetisation curves of the films were collected using a KLA Tencor model 10 vibrating sample magnetometer (VSM).

4. Variations in reflectivity across a post-oxidised iron oxide thin film deposited on MgO

The first iron oxide thin film under consideration was grown by molecular beam epitaxy (MBE) in York by the authors using a post-oxidation technique. A 20 nm iron film was deposited at 1.5 Åmin^{-1}. The film was then subsequently annealed in an atmosphere of molecular oxygen at a partial pressure of 5×10^{-5} mbar at $320\,°C$. The sample was annealed at this temperature for 15 min after deposition was completed. The samples are unpatterned and intended to be uniform.

Ten reflection spectra were recorded at different positions on the sample, with a spot diameter of 20 µm. The first seven spectra were taken in a line along the length of the sample, with a point separation of 0.1 mm. To test that this was representative of the rest of the sample, three additional spectra were obtained from another part of the sample 1 mm away, which were also separated by 0.1 mm. A diagram of this map is given in Fig. 1a.

Fig. 1b shows the ten reflection spectra, normalised to a gold background spectrum. It can be seen that there is little variation between the spectra, suggesting that the sample has a uniform composition across a large area. There is no significant spectral feature at any of the locations indicated. There are some small contaminant peaks beyond 600 cm^{-1} but otherwise the spectra are all very similar and very flat.

The magnetic hysteresis loop for the sample annealed for 15 min is given in Fig. 2. The loop has a very low (<50 Oe) coercivity and a large remanent magnetisation, characteristic of an iron hysteresis loop. This loop suggests that the magnetic behaviour of the sample is being dominated by the metallic iron in the film. This argument is supported by the TEM micrograph in Fig. 3. The micrograph shows that this region of the film is ~70% iron which has not been oxidised, while there is a layer of Fe_3O_4 on the surface, comprising 30% of the total film. It is important to note that the micrograph shows only ~ 22 nm of the sample laterally, which is two orders of magnitude lower than the resolution of the IR microscope, so gives very localised information.

Using the multilayer reflectivity model described in Section 2 the reflectivity of the sample was simulated, shown in Fig. 4. The simulation assumes the 70% Fe and 30% Fe_3O_4 split indicated by the TEM data. Reflectivity spectra where the film is composed
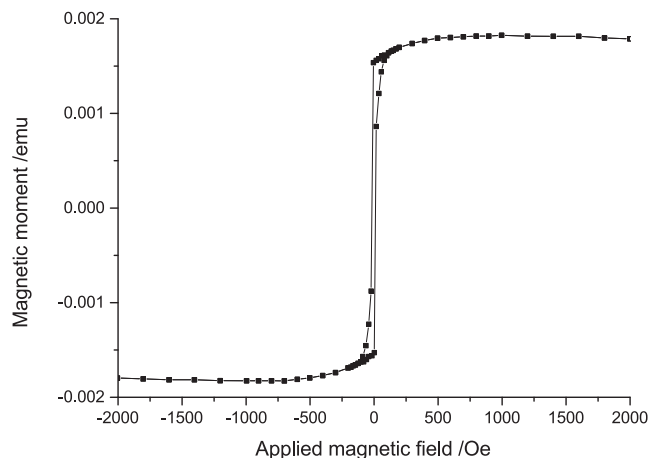
Fig. 2. Magnetometry data for the sample annealed for 15 min. The hysteresis loop has a low coercivity and high remanence, indicating that the signal produced is dominated by the presence of iron in the film.
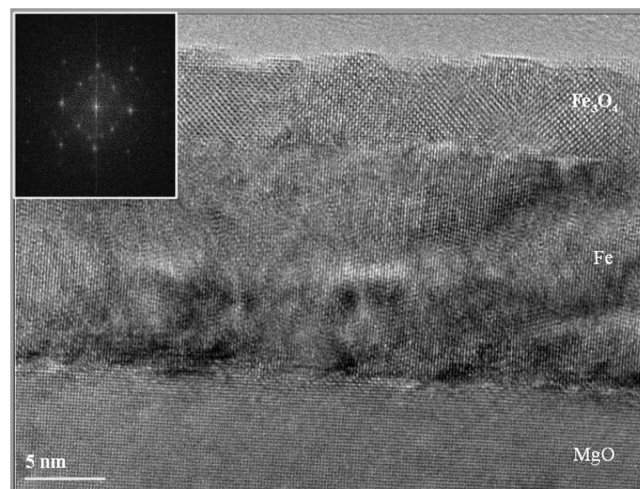
Fig. 3. TEM micrograph showing the sample annealed for 15 min is 70% unoxidised iron with a small layer of Fe_3O_4 at the surface. The inset diagram is the electron diffraction pattern of the surface layer and is of Fe_3O_4.
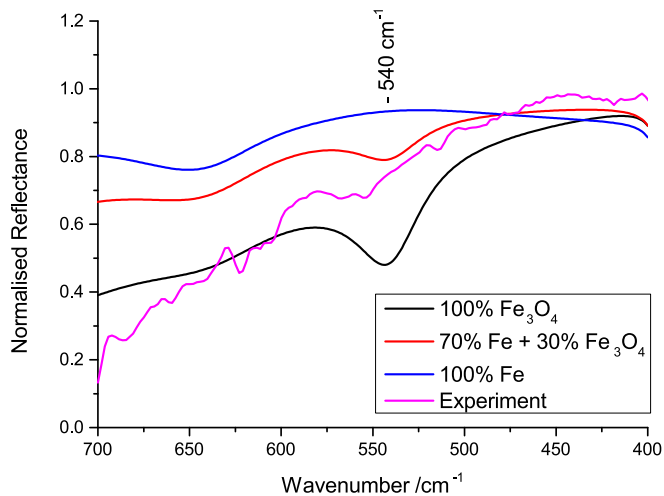
Fig. 4. Simulated reflectivity spectrum of the sample annealed for 15 min (70% iron + 30% Fe_3O_4). The Fe_3O_4 absorption at 540 cm^{-1} is very weak in the simulated spectrum, suggesting that at this sample thickness and iron/Fe_3O_4 ratio the iron reflectivity is washing out the reflectivity contribution of the oxide.

entirely of iron and entirely of Fe_3O_4 are presented on the same plot for comparison. The simulated spectrum of the sample is largely featureless, consistent with the experimental spectra; the Fe_3O_4 spectral feature is very weak in the simulation, in agreement with the prediction that the presence of a large quantity of iron would wash out the reflectivity contribution of the oxide at the surface. The general trend of decreasing reflectivity beyond 600 cm^{-1} is seen in both the experimental and simulated spectra, although much more pronounced in the experimental data.

5. Variations in reflectivity across an iron oxide thin film deposited on MgO via simultaneous oxidation

Another iron oxide thin film was grown by MBE in York by the authors, by simultaneous oxidation. A 60 nm iron film was deposited at 1.1 Åmin^{-1} in an atmosphere of molecular oxygen at a partial pressure of 5×10^{-5} mbar at 320 °C. As the iron is continuously exposed to oxygen from the beginning of the depo-

sition it is expected that the film will be oxidised down to the substrate and not just the first 3 nm. A map of reflectivity was produced of the sample as shown in Fig. 5a, where each point in the 5×5 grid is separated from its neighbours by 125 μm with a spot size of 20×20 μm. The reflectivity spectra are presented in Fig. 5b.

It can be seen that there is significant microscale variation in reflectivity across the sample indicating that there is a spatial variation in the composition of the film. There is a strong absorption in the spectra at ~ 550 cm^{-1}, which is near a characteristic phonon resonance of both maghemite and magnetite. The absorptions are all located in the same position, within the spectral resolution of the measurement, suggesting that in this region of the sample there is a mixture of maghemite and magnetite. Except for the location of the phonon absorption the reflection spectra of maghemite and magnetite are similar. The variation in the depth of the feature is therefore predicted to come from a variation in the ratio of oxidised to unoxidised iron, with the spectra becoming flatter the more iron is present.

Taking the spectra obtained for the simultaneously oxidised sample, the percentage difference between each spectra and the spectra at point P21 (chosen arbitrarily) were taken to highlight spectral variations. The percentage differences between the spectra, shown in Fig. 6, show that there is a variation in the depth of the absorption peak across the sample, but not in its position. This suggests that the ratio of magnetite to maghemite is reasonably constant across the sample, with a variation in the relative amount of iron to iron oxide.

The reflectivity of the sample at point 21 was simulated using the model outlined previously in Section 2 (point 21 was chosen as it was the spectrum being used to calculate the percentage difference between the spectra). To model the reflectivity, the ratio of magnetite to maghemite was varied in order to fit the position of the absorption feature. Once the ratio of the oxides was determined, the ratio of iron to iron oxide was used to fit the depth of the spectral feature.

5.1. Estimating the ratio of magnetite to maghemite

The simulated spectra in Fig. 7 demonstrate that if the ratio of magnetite to maghemite is varied then the position of the absorption features does move. The correct position for the spectral feature is
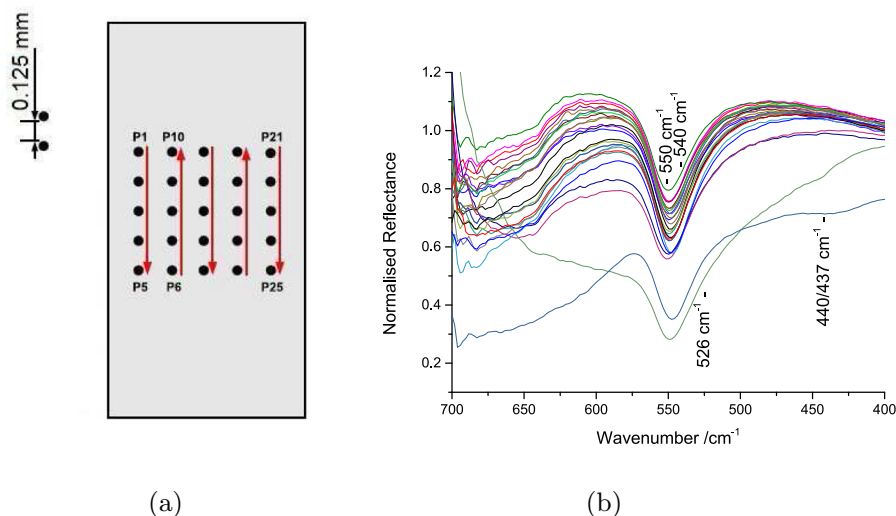

(a)

(b)

Fig. 5. a) Data collection scheme for the simultaneously-oxidised Fe_3O_4 sample. b) 25 reflection spectra taken in a 0.5×0.5 mm^2 grid with a 125 μm point separation. There is significant variation in reflectivity across the sample. The spectra with deeper absorption features are shifted towards 540 cm^{-1}, where an Fe_3O_4 phonon absorption is expected. This suggests that there is magnetite present in this area of the sample and that the ratio of magnetite to maghemite varies spatially.
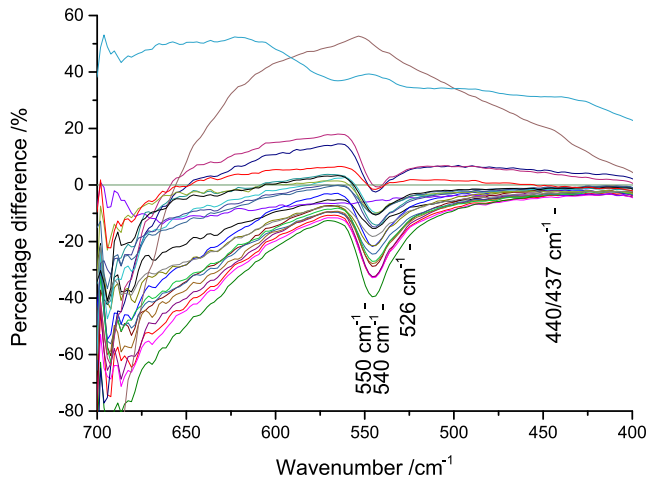
Fig. 6. Percentage difference between each spectra and the spectrum at point P21 for the simultaneous oxidation sample. There is a significant variation in the depth of the absorption feature but not its position. This suggests that the ratio of magnetite to maghemite does not vary but there is a variation in the ratio of iron to iron oxide across the sample.
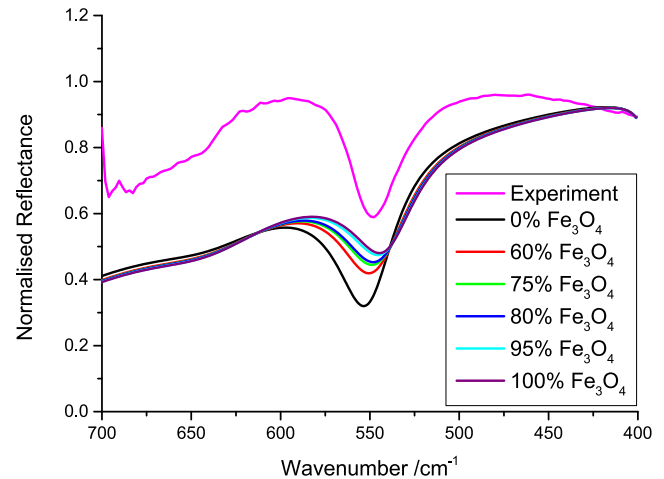

Fig. 7. Simulated reflection spectra with different ratios of magnetite to maghemite. The position of the absorption feature is dependent on the ratio of the concentration of each oxide present. The position of the feature in the experimental spectrum is reproduced when the ratio is 75% Fe_3O_4 and 25% $\gamma - Fe_2O_3$.

achieved for a sample that is 75% Fe_3O_4 and 25% γ-Fe_2O_3. It must be noted that changing the ratio of magnetite or maghemite also changes the depth of the spectral feature. This effect can be ignored in fitting the ratio of iron to iron oxide however as it has been shown that the ratio of the two oxides is not changing, so the effect must be purely due to the variation in the ratio of iron to iron oxide.

5.2. Estimating the ratio of iron oxide to iron

The ratio of iron oxide to iron was used to fit the magnitude of the absorption feature, as per Eq. (12). The simulated spectra in Fig. 8 show the variation in the depth of the absorption feature with the ratio of iron to iron oxide. The experimental depth of the spectral feature is best reproduced by a simulation with 65% oxide and 35% iron. This gives Fe(35%)γ-Fe_2O_3(15%)Fe_3O_4(50%) as an approximate composition for this point in the sample.

5.3. Modelling the differences in reflectivity as a variation in iron to iron oxide ratio

In Fig. 6 the percentage difference between the spectra and the spectrum at P21 showed that there was no shift in the position of the spectral feature, so in the modelling of the differences between the spectra the ratio of iron to iron oxide was used to generate the variation. Fig. 9 shows the percentage difference between the experimental spectra and the spectrum at P21. There are three simulated spectra; the difference between the simulated P21 spectrum and simulations of films with 40, 20 and 10% oxide content. The ratio of magnetite to maghemite has been kept constant in these simulations. The trend of the difference can be reproduced by varying the ratio of iron to iron oxide from 65%/35% to 80%/20%. This is a large variation in composition and would certainly lead to unwanted device properties.

5.4. Reflectivity variation across an iron oxide thin film deposited on an yttrium stabilised zinc oxide substrate

An Fe_3O_4 thin film was deposited using pulsed laser deposition (PLD) by Dr. Kosuke Matsuzaki of the Tokyo Institute of Technology, Japan. A KrF laser was used to ablate a sintered Fe_3O_4 target onto an yttrium stabilised zinc oxide (YSZ) substrate. 100 nm of Fe_3O_4 was deposited in 2×10^{-6} mbar partial pressure of molecu-
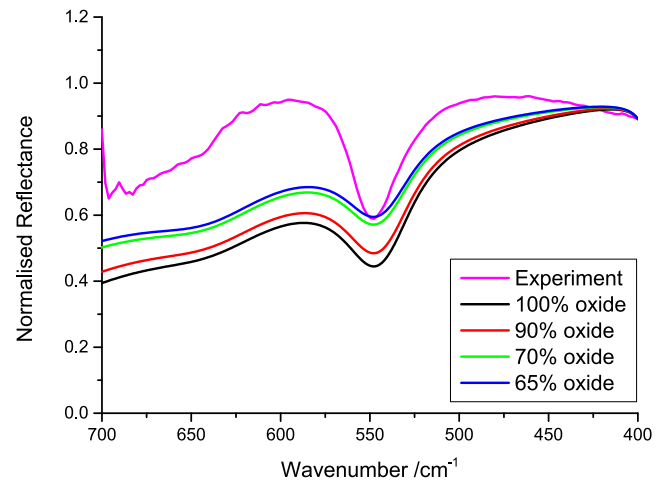

Fig. 8. Simulated spectra with different ratios of iron oxide to iron. The depth of the absorption feature in the experimental spectrum is reproduced with 65% oxide and 35% iron.
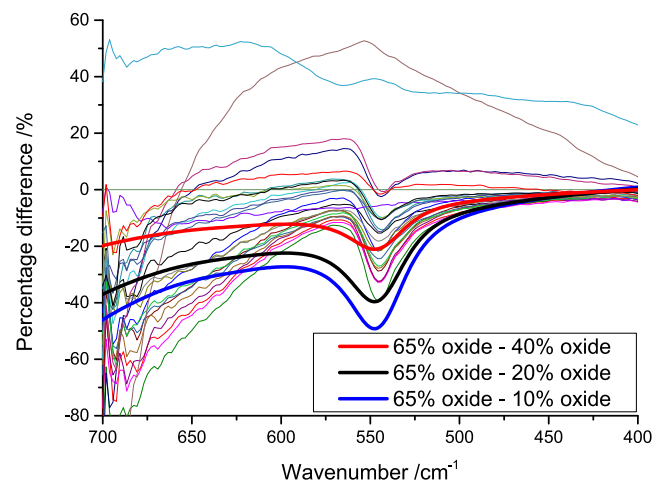

Fig. 9. Percentage difference between the experimental spectra and the spectrum at P21 for the medium map. The percentage difference between the simulated P21 spectrum and spectra with lower oxide content are also shown, demonstrating that varying the iron to iron oxide concentration reproduces the experimental trend.

lar oxygen at 300 °C. The sample was subsequently annealed in 2×10^{-6} mbar at 1200 °C. The sample is unpatterned so it was expected to be uniform.

Six reflection spectra were recorded at different positions on the sample, with a spot diameter of 20 μm. The spectra were taken in a line along the length of the sample, with each spectrum separated from its neighbours by 0.1 mm. A diagram of this linescan is given in Fig. 10a.

Normalising the spectra to the gold reference spectrum produces the six spectra shown in Fig. 10b. It can be seen that there is little to no variation in reflectivity across the sample, suggesting it is highly uniform. There is a strong absorption at 542 cm^{-1}, the location of a phonon mode in Fe_3O_4. These spectra suggest that the film consists primarily of Fe_3O_4 with almost no contaminant oxide present. The IR microspectroscopy for this sample suggests that this Fe_3O_4/YSZ thin film is composed of Fe_3O_4 and is highly uniform, making it ideal for spintronic applications.

The TEM micrograph in Fig. 11 was obtained by Dr. Vlado Lazarov and Dr. Leonardo Lari and is reproduced from the work of Matsuzaki et al. [19]. The micrograph clearly shows a highly uniform Fe_3O_4 structure down to the atomically sharp interface with the substrate. This confirms the observation in the IR spectroscopy that there is no variation across the sample and it is comprised of highly uniform Fe_3O_4.

6. Conclusions

Chemical variations across three iron oxide thin films were measured by collecting reflectivity spectra, obtained at the SOLEIL synchrotron, in an attempt to determine the composition of the samples and observe any spatial variations in reflectivity, which could be linked back to the film structure. One film each was produced by post-oxidation, simultaneous oxidation and PLD. The reflectivity spectra observed demonstrated that the post-oxidised films were 70% iron with an Fe_3O_4 layer at the surface, contributing to 30% of the films thickness, in agreement with the theory regarding their preparation. Simulated reflection spectra with this composition ratio, magnetometry and TEM all support this conclusion. There was significant variation in reflectivity across the simultaneously-oxidised sample over a large area and with a
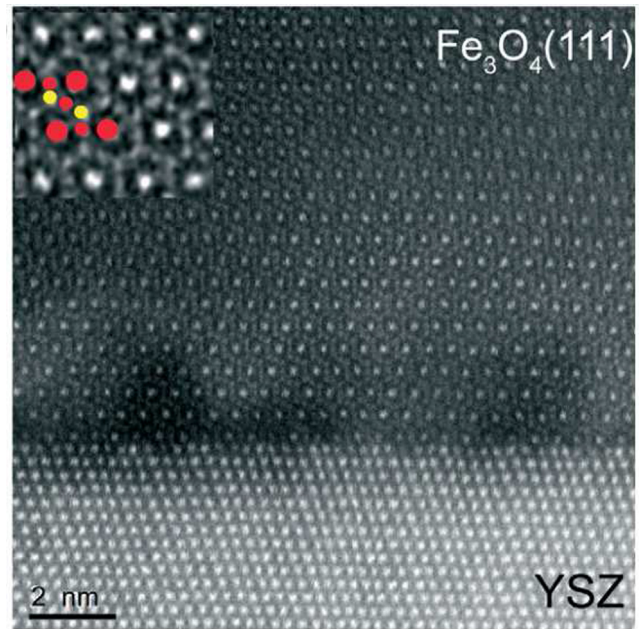

Fig. 11. TEM micrograph of the Fe_3O_4/YSZ thin film, reproduced from the work of Dr. Kosuke Matsuzaki [19]. The micrograph shows the Fe_3O_4 film is uniform and free of contaminant phases up to the atomically sharp interface with the YSZ substrate.

resolution near the resolving limit of the IR microscope. Through modelling the variation in the reflectivity the composition of the sample at the reference point was estimated to be Fe (35%)γ-Fe_2O_3(15%)Fe_3O_4(50%). The trends in the variation of reflectivity across the sample could be reproduced by varying the ratio of iron to iron oxide from 65%/35% to 80%/20%, while keeping the ratio of Fe_3O_4 to γ-Fe_2O_3 constant. There was no reflectivity variation observed across the sample deposited by PLD and all the spectra showed a strong Fe_3O_4 absorption feature, strongly indicating the sample is highly uniform Fe_3O_4. The TEM data confirmed the IR microspectroscopy observations, showing a highly ordered Fe_3O_4 film down to an atomically sharp substrate.
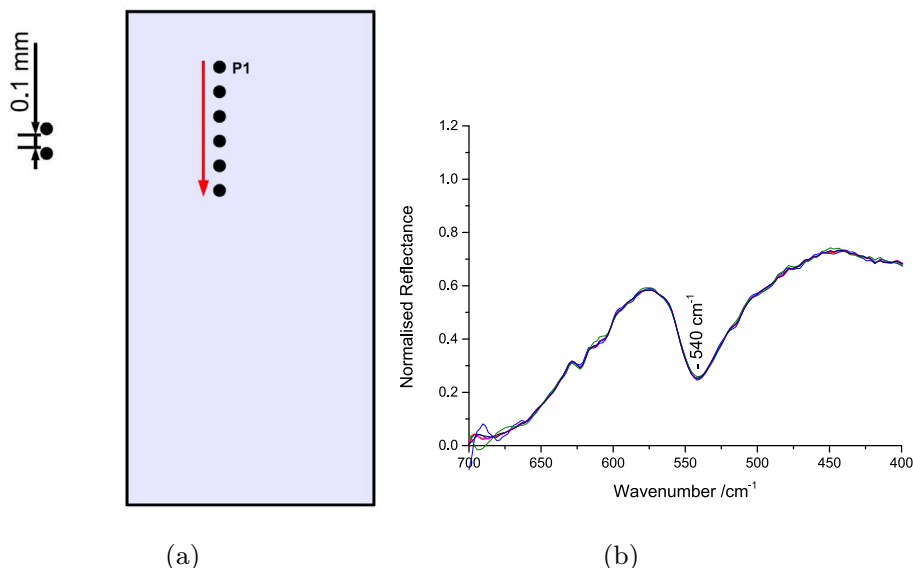

(a)   (b)

Fig. 10. a) Linescan schematic showing the positions of the six reflection spectra recorded from the Fe_3O_4/YSZ thin film. b) Normalised reflection spectra taken from the Fe_3O_4/YSZ thin film. There is a very strong absorption at 542 cm^{-1} indicating the film is composed of Fe_3O_4.

In summary, post oxidation has been shown to produce an oxide layer of limited thickness, although such a layer was shown to be uniform across the sample. This suggests post oxidation is only useful for growing Fe_3O_4 films thinner than 5 nm. Simultaneous oxidation was shown to produce a film which is predominantly oxidised but to more than one oxide phase, with the amount of oxidation varying across the sample. This suggests that it may be possible to grow Fe_3O_4 by this technique but not with the growth conditions used. A systematic study of various growth conditions must be undertaken to determine conclusively if this technique can produce device quality films. PLD was shown to produce high quality, uniform films.

IR microspectroscopy accompanied by modelling of the complex dielectric function was demonstrated to be capable of estimating the film composition, as well as detecting the spatial variation in the composition across the samples in a straightforward and non-destructive measurement. In all three of these very different cases, IR microspectroscopy proved an excellent indicator of both film composition and film quality, demonstrating it is a very powerful technique for characterising complex magnetic oxide thin films.

Acknowledgements

References

[1] D.J. Huang, C.F. Chang, H.-T. Jeng, G.Y. Guo, H.-J. Lin, W.B. Wu, H.C. Ku, A. Fujimori, Y. Takahashi, C.T. Chen, Spin and orbital magnetic moments of Fe_3O_4, Phys. Rev. Lett. 93 (2004) 077204, http://dx.doi.org/10.1103/PhysRevLett.93.077204.

[2] A. Yanase, N. Hamada, Electronic structure in high temperature phase of Fe_3O_4, J. Phys. Soc. Jpn. 68 (1999) 1607–1613, http://dx.doi.org/10.1143/JPSJ.68.1607.

[3] R. Arras, L. Calmels, B. Warot-Fonrose, Electronic structure and interface states at the Fe_3O_4/MgO(100) interface, J. Phys: Conf. Ser. 200 (2010) 072008, http://dx.doi.org/10.1088/1742-6596/200/7/072008.

[4] R. Arras, B. Warot-Fonrose, L. Calmels, Electronic structure near cationic defects in magnetite, J. Phys.: Condens. Matter 25 (2013) 256002, http://dx.doi.org/10.1088/0953-8984/25/25/256002.

[5] M. Fonin, Y.S. Dedkov, R. Pentcheva, U. Rüdiger, G. Güntherodt, Magnetite: a search for the half-metallic state, J. Phys.: Condens. Matter 25 (2013) 256002, http://dx.doi.org/10.1088/0953-8984/19/31/315217.

[6] G.E. Sterbinsky, J. Cheng, P.T. Chiu, B.W. Wessels, D.J. Keavney, Investigation of heteroepitaxial growth of magnetite thin films, J. Vac. Sci. Technol. B 25 (2007) 1389–1392, http://dx.doi.org/10.1116/1.2757185.

[7] C.S. Kelley, J. Naughton, E. Benson, R.C. Bradley, V.K. Lazarov, S.M. Thompson, J.A.D. Matthew, Investigating the magnetic field-dependent conductivity in magnetite thin films by modelling the magnetorefractive effect, J. Phys.: Condens. Matter 26 (3) (2014) 036002, http://dx.doi.org/10.1088/0953-8984/26/3/036002.

[8] A.M. Jubb, H.C. Allen, Vibrational spectroscopic characterization of hematite, maghemite, and magnetite thin films produced by vapor deposition, Appl. Mater. Interfaces 2 (2010) 2804–2812, http://dx.doi.org/10.1021/am1004943.

[9] C.S. Kelley, S.M. Thompson, M.D. Illman, S. LeFrançois, P. Dumas, Spatially resolving variations in giant magnetoresistance, undetectable with four-point probe measurements, using infrared microspectroscopy, Appl. Phys. Lett. 101 (2012) 162402, http://dx.doi.org/10.1063/1.4760282.

[10] E. Hecht, Optics, 4th Edition., Addison Wesley, 2002.

[11] C. Kittel, eigth ed., Introduction to Solid State Physics, Wiley, 2005.

[12] P.W. Anderson, Antiferromagnetism. theory of superexchange interaction, Phys. Rev. 79 (1950) 350–356, http://dx.doi.org/10.1103/PhysRev. 79.350.

[13] L. Degiorgi, P. Wachter, D. Ihle, Small-polaron conductivity in magnetite, Phys. Rev. B 35 (1987) 9259–9264, http://dx.doi.org/10.1103/PhysRevB.35.9259.

[14] J.S. Ahn, H.S. Choi, T.W. Noh, Infrared reflectance studies on a Fe_3O_4 film deposited on a MgO substrate: Observation of the substrate longitudinal optic phonon resonance peak in the film geometry, Phys. Rev. B 53 (1996) 10310–10316, http://dx.doi.org/10.1103/PhysRevB.53.10310.

[15] J.D.E. McIntyre, D.E. Aspnes, Differential reflection spectroscopy of very thin surface films, Surf. Sci. 24 (1971) 417–434, http://dx.doi.org/10.1016/0039-6028(71)90272-X.

[16] C.S. Kelley, Spatially Resolved Infrared Spectroscopy For Spintronics (Ph.D. thesis), University of York, 2014, URL http://etheses.whiterose.ac.uk/id/eprint/6589.

[17] S.S. Aplesnin, G.I. Barinov, Pressure-induced orbital ordering in magnetite above the verwey temperature, Phys. Solid State 49 (2007) 1949–1952, http://dx.doi.org/10.1134/S1063783407100228.

[18] N.F. Mott, The resistance, The resistance and thermoelectric properties of the transition metals, Proc. R. Soc. London Ser. A, Math. Phys. Sci. 156 (1936) 368–382, http://dx.doi.org/10.1098/rspa.1936.0154.

[19] K. Matsuzaki, V.K. Lazarov, L. Lari, H. Hosono, T. Susaki, Fe_3O_4(1 1 1) thin films with bulk-like properties: growth and atomic characterization, J. Phys. D: Appl. Phys. 46 (2013) 022001, http://dx.doi.org/10.1088/0022-3727/46/2/022001.